

Study of the Enzyme-Free Glucose Biosensor Based on Ni²⁺@ Poly (Neutral Red) Hybrid Nanocomposites (Ni²⁺@PNR HN)/MWCNTs/Nafion Modified Electrode

Zheng Chang* and Zhuanzhuan Gao

Department of Applied Chemistry of College of Science, Xi'an University of Technology, Xi'an 710054, P.R. China

*E-mail: czheng@xaut.edu.cn

Received: 28 September 2017 / Accepted: 22 November 2017 / Published: 28 December 2017

In this paper, we concentrated on the simplest way to synthesize Nickel ion doped poly (neutral red) (Ni²⁺@PNR) hybrid nanocomposites (abbreviated as Ni²⁺@PNR HN) through a reverse microemulsion method. Because the MWCNTs/Nafion composite film was negatively charged, the positively charged Ni²⁺@PNR HN can be adsorbed by electrostatic interactions onto the surface of MWCNTs/Nafion modified electrode. The hybrid nanocomposite exhibited excellent electrocatalytic activity for glucose oxidation due to three-in-one synergistic effects, namely, the special copolymerization structures of Ni²⁺@PNR HN as an active catalytic center; the amount of doping of Ni²⁺ can be tuned by the attachment of NR with MWCNTs/Nafion, resulting in the hybrid nanocomposites containing much more Ni²⁺ and possessing a significant signal amplification effect toward the glucose oxidation reaction; the effective immobilization of Ni²⁺ at the modified electrode surface was achieved by the non-covalent interaction of hybrid nanocomposites and MWCNTs/Nafion support materials. Accordingly, the Ni²⁺@PNR HN/MWCNTs/Nafion modified electrode displayed an enhanced electrocatalytic activity to glucose oxidation in 0.1 mol·L⁻¹ NaOH solution, owning the advantages of higher sensitivity, lower detection limit, wide linear range, and good stability and selectivity for constructing a novel enzyme-free glucose electrochemical sensor.

Keywords: Ni²⁺@poly (neutral red) hybrid nanocomposites (Ni²⁺@PNR HN); MWCNTs/Nafion modified electrode; enzyme-free glucose biosensor

1. INTRODUCTION

Glucose, a chemical formula C₆H₁₂O₆, is the most widely distributed and important monosaccharide in nature. Glucose plays an important role in the field of biology. It is the energy source and metabolic intermediate product of living cells, that is, the main energy supply of biological

energy. The development of a fast and reliable method for rapid determination of glucose concentration is of great significance in clinical diagnosis. The development of electrochemical glucose sensors has attracted considerable attention over the past few years [1-3]. Commonly, the electrochemical detection of glucose is carried out on the basis of the glucose oxidase (GOx) enzyme, however, enzyme-modified electrodes have several disadvantages, such as high enzyme costs, instability, complicated immobilization procedures and critical operating conditions, etc [4-6].

In order to resolve these problems, a great amount of research has been devoted to fabricating an enzyme-free glucose sensor [7-10]. Among these, metal nickel-based compounds exhibit remarkable electrocatalytic abilities for glucose due to their exclusive redox behavior ($\text{Ni}^{2+}/\text{Ni}^{3+}$), high surface to electroactive area, and biocompatibility [11-12]. However, pure metal of Ni is difficult to prepare and have poor stability for electroanalysis because it's readily oxidized in air and in solution [13]. In recent years, many studies have been devoted to the synthesis of different morphologies of Nickel, such as nanoparticles, nanorods, nanosheets, nanowires, nanoplates, mesoporous structures and hollow nanospheres, especially by the support of carbonaceous materials [14-20]. Therefore, it is still necessary to propose a simple and one-step synthesis method to prepare nickel based nanomaterials, which will be applied to the research of novel nonenzymatic glucose electrochemical sensors.

On the other hand, the existing methods for immobilization of Nickel-based materials include electrochemical polymerization [21-22], direct electrodeposition [23-24], electrostatic adsorption [25], electrospinning [26], thermal catalytic etching technique [27] and sol-gel method [28], etc. However, due to the poor permeability of polymer film, the sensitivity and stability of the polymer film modified electrode produced by polymerization will be reduced; the direct deposition requires complex instruments and the sediments are unstable; the Nickel-based materials by electrostatic adsorption is generally small amount, easy to fall off, lost in the solution; the electrospinning and thermal catalytic etching technique are suffering from some disadvantages, such as extremely long and costly processes as well as complexity; the sol-gel method makes the electrical activity of molecule easily restricted by the conductivity of the substrate. Therefore, there is an urgent need to develop a new method for immobilization of Nickel-based materials on electrodes.

Carbon materials have been used as a matrix to enhance electron transfer rates and electrocatalytic activities. As one important carbon material, the unique properties of carbon nanotubes (CNTs), such as remarkable surface area, excellent conductivity, and wide electrochemical range, make it an ideal material in electrochemical sensors [29-30]. In addition, Nafion is an excellent cation exchange agent, composed of a perfluorinated sulfonic acid ester, and the composite film of Nafion and CNTs which can be easily attracted by ion exchange process, hydrophobic interaction and electrostatic adsorption of hydrophobic cations, such as Ni^{2+} [31-32]. Furthermore, Neutral red (NR) is a kind of living as a cell staining and pH indicator of basic phenazine dye and its monomer on the conductive substrate with good electrochemical behavior, which has a good catalytic effect on some biological molecules [33-34]. NR has been reported to be good electronic mediator in monomer form also but the main problem working with monomer NR is that it leaches out from immobilization matrix at electrode surface. So the attachment of NR with MWCNTs and Nafion needs to be highly deliberate.

In this paper, we concentrated on the simplest way to synthesize the Ni²⁺@ poly (neutral red) hybrid nanocomposites (Ni²⁺@PNR HN) through a reverse microemulsion method. Because the MWCNTs/Nafion composite film was negatively charged, the positively charged Ni²⁺@PNR HN can be adsorbed by electrostatic interactions onto the surface of MWCNTs/Nafion modified electrode. Three-in-one synergistic effects existed simultaneously, namely, the special copolymerization structures of Ni²⁺@PNR HN as an active catalytic center; the amount of doping of Ni²⁺ can be tuned by the attachment of NR with MWCNTs/Nafion, resulting in the hybrid nanocomposites containing much more Ni²⁺ and possessing a significant signal amplification effect toward the glucose oxidation reaction; the effective immobilization of Ni²⁺ at the modified electrode surface was achieved by the non-covalent interaction of hybrid nanocomposites and MWCNTs/Nafion support materials. Furthermore, we proposed the possible mechanism of the formation of Ni²⁺@PNR HN. The as-prepared hybrid nanocomposites were confirmed by various physical characterizations and the practicality of the proposed glucose sensor was also demonstrated toward glucose detection in injection and human serum samples with satisfactory results.

2. EXPERIMENTAL

2.1 Instruments and reagents

All electrochemical tests were performed by using a CHI660E electrochemical working station (Chen Hua Inc., China). A RO•5•S025 multi-position magnetic stirrer (IKA, Germany) and TG16G centrifuges (Xi'an Mogina Instruments Manufacturing Co., Ltd.) were all used for the synthesis of Ni²⁺@PNR HN. Fluorescence spectra were recorded on a Hitachi F-7000 fluorescence spectrophotometer (Hitachi, Japan). And, the Ni²⁺@PNR HN was characterized by a JEM-2100 transmission electron microscope (TEM, Hitachi Electronics Corporation, Japan), Merlin Compact field emission scanning electron microscope (SEM, Carl Zeiss, Germany) and IR Prestige-21 transform infrared spectrometer (Shimadzu, Japan). All experiments were carried out with a conventional three-electrode system in a 10 mL electrochemical cell. A glass Carbon electrode (GCE) with 3 mm in diameter was used as the basic working electrode, and a twisted platinum wire was used as the counter electrode. All the potentials quoted here were relative to an Ag/AgCl (saturated KCl) reference electrode.

Multi-walled Carbon nanotubes (MWCNTs, Shanghai Aladdin Chemical Reagent Co. Ltd., China) and Nafion 117 (5 % in a mixture of lower aliphatic alcohols and water, DuPont Co. of U.S.A.) were prepared of MWCNTs/Nafion dispersion with a concentration of 0.2 mg·mL⁻¹. Nickel nitrate was purchased from Xi'an Chemical Reagent Factory, China. And, Neutral red (NR) was purchased from Tianjin Hebei District Haijing Fine Chemical Factory, China. Urea acid (UA, Chinese, Wu Sanhua factory packaging, packaging of goods in Hungary), and ascorbic acid (AA) and dopamine (DA) were purchased from Shanghai Aladdin Chemical Reagent Co. Ltd., China. Stock standard solutions of glucose (Tianjin Hengxing Chemical Reagent Co. Ltd., China) were prepared by dissolving appropriate amount of glucose in 0.1 mol·L⁻¹ NaOH at a concentration of 0.1 mol·L⁻¹ and stored at 4 °C. Glucose injection produced by Sichuan Kelun pharmaceutical Co. Ltd., China. Fresh human serum

samples are provided by Xi'an University of Technology hospital. All reagents were of analytical reagent grade without further purifications, and doubly distilled water was used throughout.

2.2 Synthesis of $Ni^{2+}@PNR\ HN$

The $Ni^{2+}@PNR\ HN$ was synthesized by the reverse microemulsion method. The reverse microemulsion system (W/O) was prepared first by mixing in agitation 1.80 mL of Triton X-100, 7.50 mL of cyclohexane and 1.80 mL of 1-hexanol for 30 min. When the mixing solution becomes clear, 250 μL of doubly distilled water was added into the mixture. After this, 100 μL of $0.02\text{ mol}\cdot\text{L}^{-1}$ NR solution and 20 μL of $0.02\text{ mol}\cdot\text{L}^{-1}$ Ni^{2+} were dripped stirringly, respectively. After 30 min, a polymerization reaction was initiated by adding 100 μL of $0.02\text{ mol}\cdot\text{L}^{-1}$ ammonium persulfate (APS). The polymerization reaction was allowed to continue for 12 h under vigorous agitation. Acetone was then added to destroy the emulsion, followed by centrifuging and washing with ethanol and water for three times, respectively. Finally, the prepared hybrid nanocomposite was dispersed in doubly distilled water and stored in $4\text{ }^{\circ}\text{C}$ refrigerator. Without adding 20 μL $0.02\text{ mol}\cdot\text{L}^{-1}$ Ni^{2+} , the PNR was obtained in the same way.

2.3 Preparation of $Ni^{2+}@PNR\ HN/MWCNTs/Nafion$ modified electrode

Prior to modification, the bare GCE was polished to a mirror-like surface using $0.3\text{ }\mu\text{m}$ and $0.05\text{ }\mu\text{m}$ alumina slurries sequentially, and then ultrasonically cleaned in water. Afterward, 30 μL $Ni^{2+}@PNR\ HN$ were dispersed in 60 μL of $0.2\text{ mg}\cdot\text{mL}^{-1}$ MWCNTs/Nafion mixed solution, and mixing appropriate amount of ethanol were ultrasonicated homogeneously for 15 min. Then, about 2 μL mixed homogeneous droplet was dropped on the surface of the well-polished GCE. After drying, the $Ni^{2+}@PNR\ HN/MWCNTs/Nafion$ modified electrode was prepared well. The modified electrodes were subjected to investigate the electrochemical behavior of electrodes and glucose oxidation.

The prepared MWCNTs/Nafion mixed solution with 3 μL was applied to the GCE surface, and the MWCNTs/Nafion modified electrode was made and dried at room temperature. Then, the MWCNTs/Nafion modified electrode was inserted into the mixing solution containing $2.0\times 10^{-5}\text{ mol}\cdot\text{L}^{-1}$ NR, $1.0\times 10^{-5}\text{ mol}\cdot\text{L}^{-1}$ Ni^{2+} and $0.1\text{ mol}\cdot\text{L}^{-1}$ PBS (pH=5.5), scan rate of $50\text{ mV}\cdot\text{s}^{-1}$, potential window of $-1.4\text{ V} \sim +1.8\text{ V}$ for 5 circles of electro-initiation, then $-0.8\text{ V} \sim +0.8\text{ V}$ for 40 circles, the $Ni^{2+}/PNR/MWCNTs/Nafion$ modified electrode was obtained by cyclic voltammetry (CV). The PNR/MWCNTs/Nafion and P- $Ni^{2+}/MWCNTs/Nafion$ modified electrodes can be prepared by the above method without Ni^{2+} or NR solution.

2.4 Experimental procedure

The electrochemical measurements of $Ni^{2+}@PNR\ HN/Nafion/MWCNTs$ modified electrode in $0.1\text{ mol}\cdot\text{L}^{-1}$ NaOH containing blank or different concentrations of glucose standard solution, such as CV and Chronoamperometry, were performed successively.

3. RESULTS AND DISCUSSION

3.1 Characterization of synthesized Ni^{2+} @PNR HN

The SEM images of Ni^{2+} @PNR HN/MWCNTs/Nafion were shown in **Fig.1**. The MWCNTs was twining (**Fig.1a**). When decorated with PNR (**Fig.1b**), it was clear that PNR had been adsorbed on the surface of MWCNTs/Nafion, and crosslinked with MWCNTs. It can be also seen that the doping of Ni^{2+} made Ni^{2+} @PNR HN and MWCNTs/Nafion form multilayer and three-dimensional spatial structure (**Fig.1c**). And, it can be distinctly seen from TEM images that the synthesized Ni^{2+} @PNR HN was scaly, with a diameter of about 20 to 30 nm (as shown in **Fig.2**).

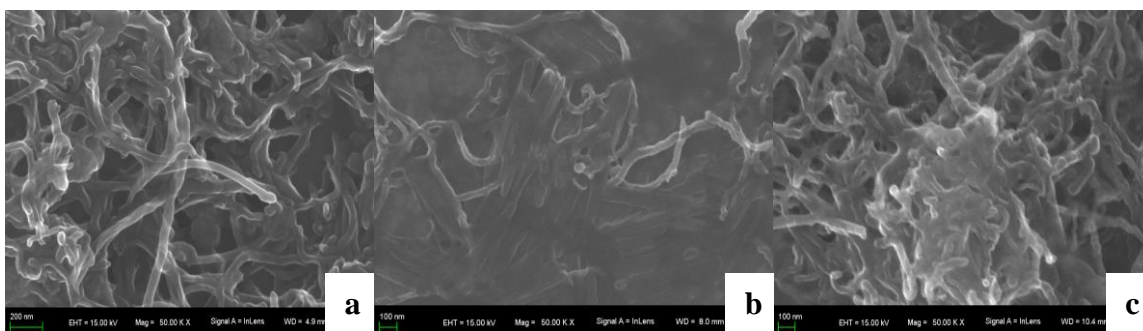


Figure 1. SEM images of Ni^{2+} @PNR HN/MWCNTs/Nafion.

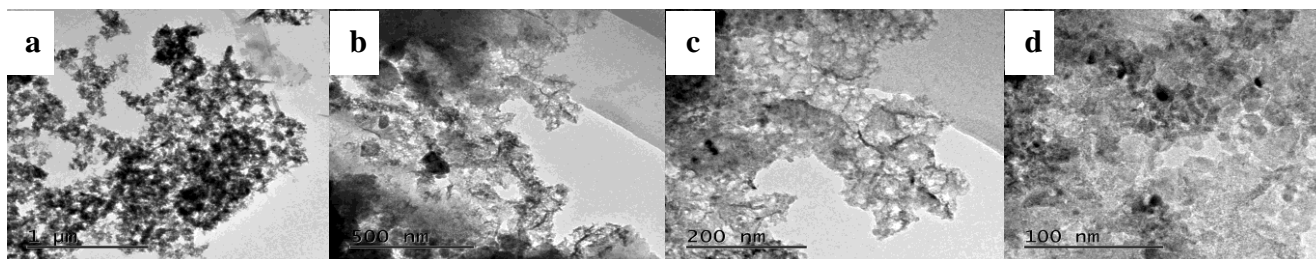


Figure 2. TEM images of Ni^{2+} @PNR HN.

The fluorescence spectra of NR solution, Ni^{2+} /NR solution and Ni^{2+} @PNR HN were shown in **Fig.3**. The maximum excitation and emission wavelengths of NR solution were 534 nm and 640 nm, respectively (**Fig.3a and 3b**). The maximum excitation and emission wavelengths of Ni^{2+} /NR solution were 535 nm and 634 nm, respectively (**Fig.3c and 3d**). Accordingly, the emission wavelength shifted blue by 6 nm. The possible reason was that Ni^{2+} and NR formed simple Nickel complex resulting in the emission wavelength to move. However, the maximum excitation and emission wavelengths of Ni^{2+} @PNR HN were at 551 nm and 600 nm (**Fig.3e and 3f**), respectively, and the maximum excitation and emission wavelengths shifted considerably. The possible reason was that when $\text{K}_2\text{S}_2\text{O}_8$ was used as an initiator, a NR cation radical was generated and collided with each other to form a dimer and further an oligomer [35]. In the process of chemical polymerization in situ, Ni^{2+} was doped

to form a hybrid nanocomposite, which resulted in the larger shift of maximum excitation and emission wavelengths.

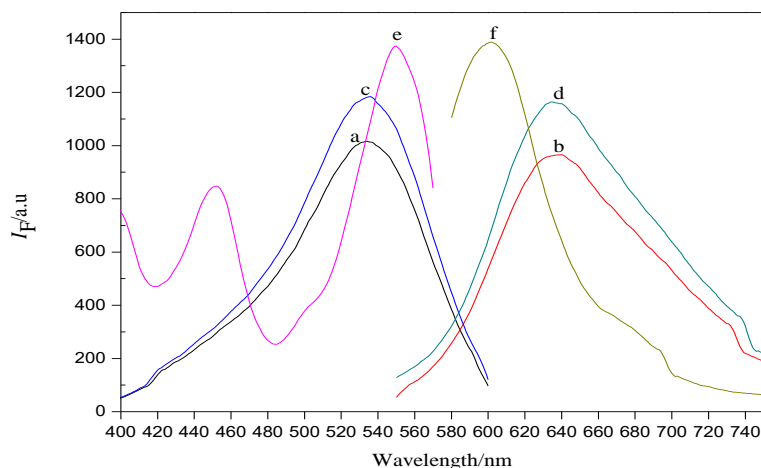


Figure 3. Fluorescence spectra of NR solution (a and b), Ni^{2+}/NR solution (c and d) and $\text{Ni}^{2+}@ \text{PNR}$ HN (e and f). ($c_{\text{NR}} = 2.5 \times 10^{-6} \text{ mol} \cdot \text{L}^{-1}$, $c_{\text{Ni}^{2+}} = 5.0 \times 10^{-7} \text{ mol} \cdot \text{L}^{-1}$)

The infrared spectra of NR solution, Ni^{2+}/NR solution and $\text{Ni}^{2+}@ \text{PNR}$ HN were shown in **Fig.4**. NR solution (**a**) was located at 1654.8 cm^{-1} , 1458.1 cm^{-1} , 1382.9 cm^{-1} and 1049.2 cm^{-1} , which was the skeleton vibration absorption peaks of benzene ring. The absorption peak of two substituent groups of benzene ring was at 881.4 cm^{-1} . The stretching vibration of C-N bond on the phenothiazine ring was located at 1330.8 cm^{-1} [36]. The plane bending vibration of C-H bond was located at 1274.9 cm^{-1} . The corresponding absorption peaks of Ni^{2+}/NR solution (**b**) were 1652.9 cm^{-1} , 1454.2 cm^{-1} , 1382.9 cm^{-1} and 1049.2 cm^{-1} , respectively. The stretching vibration of C-N bond was located at 1330.8 cm^{-1} . The plane bending vibration of C-H bond was located at 1276.8 cm^{-1} . The absorption peaks corresponding to $\text{Ni}^{2+}@ \text{PNR}$ HN (**c**) were 1649 cm^{-1} , 1456.1 cm^{-1} , 1382.9 cm^{-1} and 1049.2 cm^{-1} , respectively. The stretching vibration of C-N bond was located at 1334.6 cm^{-1} . The plane bending vibration of C-H bond was located at 1278.7 cm^{-1} . Compare to NR monomer (**a**) or Ni^{2+}/NR solution (**b**), the C=C or C=N stretching vibration on the benzene ring of $\text{Ni}^{2+}@ \text{PNR}$ HN (**c**) was blue shifted by 3.9 cm^{-1} , the C-N stretching vibration was red shifted by 3.8 cm^{-1} , and C-H plane bending vibration shifted by 3.8 cm^{-1} , respectively. The displacement effect was attributed to the relaxation of the conjugated structure of hybrid polymers caused by the doping of Ni^{2+} . After NR chemical polymerization, the degree of conjugation in the whole molecular structure was increased, but due to the doping of Ni^{2+} , the degree of conjugate structure was less than that reported in the literature [37].

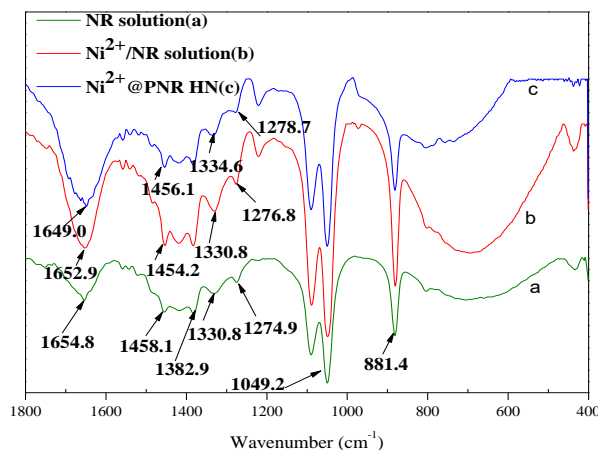


Figure 4. Infrared spectrograms of NR solution (a), Ni²⁺/NR solution (b) and Ni²⁺@PNR HN (c).

3.2 The electrochemical behavior of Ni²⁺@PNR HN/MWCNTs/Nafion modified electrode

3.2.1. The electrochemical behaviors of PNR/MWCNTs/Nafion, P-Ni²⁺/MWCNTs/Nafion and Ni²⁺/PNR/MWCNTs/Nafion modified electrode

CV curves of three prepared modified electrodes in 0.1 mol·L⁻¹ NaOH solution were shown in **Fig.5**. Under alkaline conditions, the PNR/MWCNTs/Nafion modified electrode (**Fig.5a**) had no electrical activity. The redox peak potentials of P-Ni²⁺/MWCNTs/Nafion modified electrode were occurred at 0.627 V and 0.466 V (**Fig.5b**), respectively, which was the typical redox wave of the couple of Ni²⁺/Ni³⁺ [38]. The Ni²⁺/PNR/MWCNTs/Nafion modified electrode showed a pair of redox peaks at 0.646 V and 0.451 V (**Fig.5c**), which corresponded to the transformation between Ni²⁺ and Ni³⁺, respectively.

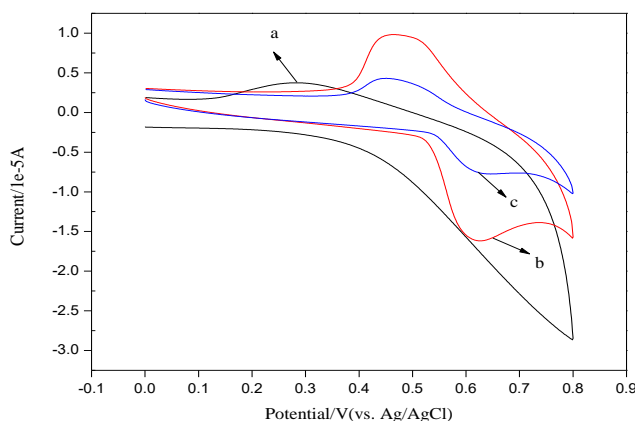


Figure 5. CV curves of the PNR/MWCNTs/Nafion(a), P-Ni²⁺/MWCNTs/Nafion(b) and Ni²⁺/PNR/MWCNTs/Nafion (c) modified electrode in 0.1 mol·L⁻¹ NaOH solution.

The results showed that, Ni^{2+} can be doped into the polymer film of PNR by electro-polymerization under alkaline conditions. Compared to the P- Ni^{2+} /MWCNTs/Nafion modified electrode, the reversibility of the Ni^{2+} /PNR/MWCNTs/Nafion modified electrode became worse, and the reversible reaction between Ni^{2+} and Ni^{3+} would be restricted by the electrochemical activity of the NR polymer film.

3.2.2 Comparison of electrochemical responses of Ni^{2+} /PNR/MWCNTs/Nafion and Ni^{2+} @PNR HN/MWCNTs/Nafion modified electrode to Glucose

A comparative study on the electrocatalytic performance toward glucose oxidation at different modified electrodes were carried out by CV (**Fig.6**). A pair of redox peaks appeared at 0.646 V and 0.451 V on the Ni^{2+} /PNR/MWCNTs/Nafion modified electrode for the primary redox couple ($\text{Ni}^{2+}/\text{Ni}^{3+}$) (**Fig.6a**). When glucose was present in the solution, the oxidation and reduction peak potentials of the Ni^{2+} /PNR/MWCNTs/Nafion modified electrode did not change apparently, and there was no corresponding increase in peak current as well (**Fig.6b**). The Ni^{2+} /PNR/MWCNTs/Nafion modified electrode didn't exhibit electrocatalytic oxidation activity towards glucose, although it was prepared in an electro-polymerization solution made of Ni^{2+} and NR at the same concentration of the synthetic hybrid nanocomposite. Due to the poor permeability of polymer film, Ni^{2+} doped PNR film by electrochemical polymerization method might block the transmission electron and influence the electrocatalytic ability of Nickel ion on glucose. On the other hand, CV curves of the Ni^{2+} @PNR HN/MWCNTs/Nafion modified electrode showed that, there was a distinct redox peak at 0.697 V and 0.493 V (**Fig.6c**), respectively, and the peak shape was better, corresponding to the oxidation or reduction process of $\text{Ni}^{2+}/\text{Ni}^{3+}$. In absence of glucose, the background current of Ni^{2+} @PNR HN/MWCNTs/Nafion modified electrode (**Fig.6c**) was higher than that of other modified electrodes (**Fig.6a**), which indicated that Ni^{2+} @PNR HN/MWCNTs/Nafion modified electrode had the highest active surface area. As can be seen from the CV curve of the Ni^{2+} @PNR HN/MWCNTs/Nafion modified electrode in $0.1 \text{ mol}\cdot\text{L}^{-1}$ NaOH containing $1.0\times 10^{-5} \text{ mol}\cdot\text{L}^{-1}$ glucose solution (**Fig.6d**), the modified electrode had a very obvious electrochemical response to glucose with an oxidation peak at 0.688 V and a reduction peak at 0.533 V. The reduction peak current (from 1.884×10^{-6} A to 1.060×10^{-5} A) and the oxidation peak current (from -1.477×10^{-5} A to -4.697×10^{-5} A) all increased dramatically, and which was the result of the catalytic oxidation of glucose by Ni^{3+} on the modified electrode surface. Moreover, the Ni^{2+} @PNR HN/MWCNTs/Nafion modified electrode showed a uniquely high net current that was approximately 3.2 times greater than those in other modified electrodes. The much higher current response of the Ni^{2+} @PNR HN/MWCNTs/Nafion modified electrode may be due to its more sterically hindered structure and a larger conducting surface area to support more active species, such as Ni^{2+} . When glucose concentration was measured, the Ni^{2+} @PNR HN was easily assembled on the surface of MWCNTs/Nafion modified electrode by electrostatic interactions to achieve the electrical signal amplification.

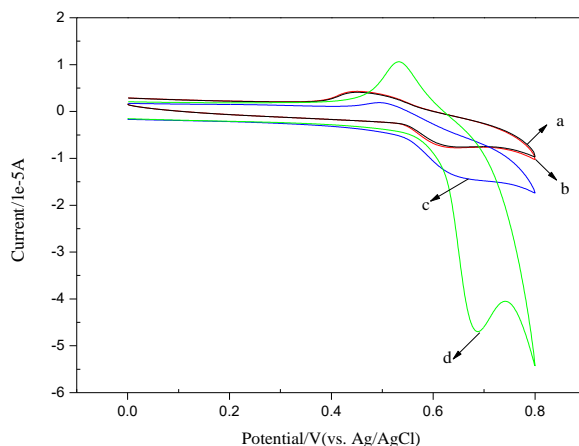


Figure 6. CV curves of the Ni^{2+} /PNR/MWCNTs/Nafion modified electrode in $0.1 \text{ mol}\cdot\text{L}^{-1}$ NaOH solution (a) and $0.1 \text{ mol}\cdot\text{L}^{-1}$ NaOH containing $1.0\times 10^{-5} \text{ mol}\cdot\text{L}^{-1}$ glucose solution (b); CV curves of the Ni^{2+} @PNR HN/MWCNTs/Nafion modified electrode in $0.1 \text{ mol}\cdot\text{L}^{-1}$ NaOH solution (c) and $0.1 \text{ mol}\cdot\text{L}^{-1}$ NaOH containing $1.0\times 10^{-5} \text{ mol}\cdot\text{L}^{-1}$ glucose solution, respectively (d).

3.2.3 Electrochemical behavior of glucose on Ni^{2+} @PNR HN/MWCNTs/Nafion modified electrode

As shown in **Fig.7a**→**e**, the Ni^{2+} @PNR HN/MWCNTs/Nafion modified electrode showed an obvious oxidation peak in $0.1 \text{ mol}\cdot\text{L}^{-1}$ NaOH solution containing different concentration of glucose at $+0.617 \text{ V}$. With the increasing of glucose concentration, the peak currents, especially the oxidation peak currents of Ni^{2+} @PNR HN/MWCNTs/Nafion modified electrode were obviously increased. The increased oxidation peak currents can be used as an electrical response signal of Ni^{2+} @PNR HN/MWCNTs/Nafion modified electrode to glucose concentration, thus realizing the high sensitive electrochemical detection of glucose concentration.

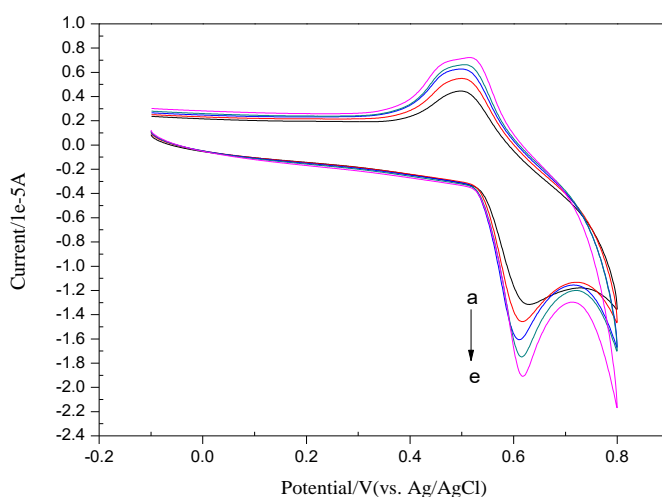


Figure 7. Electrochemical responses of different concentration of glucose on the Ni^{2+} @PNR HN/MWCNTs/Nafion modified electrode. (The concentration ranged from a → e, followed by 0, 1.0×10^{-9} , 1.0×10^{-8} , 1.0×10^{-7} , $1.0\times 10^{-6} \text{ mol}\cdot\text{L}^{-1}$.)

3.3 Optimization of experimental conditions

3.3.1 Selection of scan rate

Fig.8 showed the CV curves of glucose oxidation on the Ni²⁺@PNR HN/MWCNTs/Nafion modified electrode at various scan rates ranging from 10 to 500 mV·s⁻¹. The anodic (*i*_{pa}) and cathodic (*i*_{pc}) peak current were increased when increasing the scan rate. Simultaneously, the oxidation peak of *E*_{pa} and the reduction peak of *E*_{pc} slightly moved in the positive or negative directions, respectively.

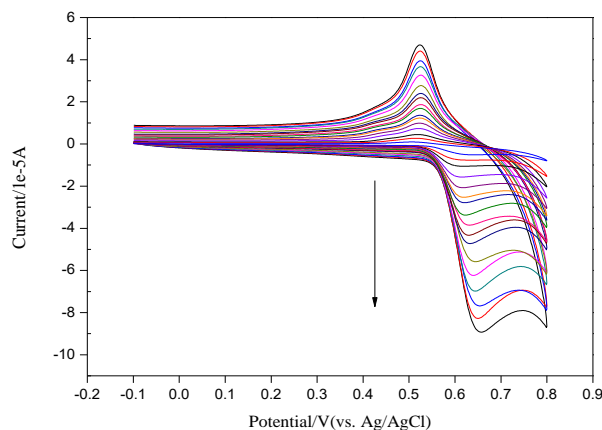


Figure 8. CV curves of the Ni²⁺@PNR HN/MWCNTs/Nafion modified electrode in 0.1 mol·L⁻¹ NaOH containing 1.0×10⁻⁵ mol·L⁻¹ glucose solution, scan rates from the inside to the outside were 10, 20, 30, 50, 70, 90, 100, 130, 150, 180, 200, 250, 300, 350, 400, 450, 500 mV·s⁻¹, respectively.

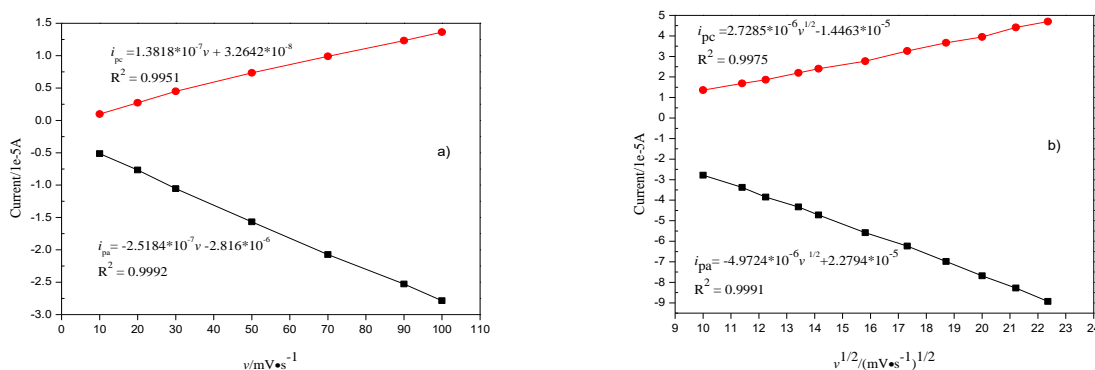


Figure 9. a) At low scan rate of 10~100 mV·s⁻¹, the linear relationship of peak current *i*_p and scan rate *v*. b) At high scan rate of 100~500 mV·s⁻¹, the linear relationship of peak current *i*_p and square root of scan rate *v*^{1/2}.

When the scan rate at low was increased from 10 mV·s⁻¹ to 100 mV·s⁻¹ (**Fig.9a**), both anodic and cathodic peak currents *i*_p were found directly proportional to the scan rates *v* with a linear equation of *i*_{pa} = -2.5184×10⁻⁷·*v* - 2.816×10⁻⁶ ($R^2 = 0.9992$) and *i*_{pc} = 1.3818×10⁻⁷·*v* + 3.2642×10⁻⁸ ($R^2 = 0.9951$), respectively. Under low scanning speed condition, the relationships between *E*_p, *i*_p and *v* showed that

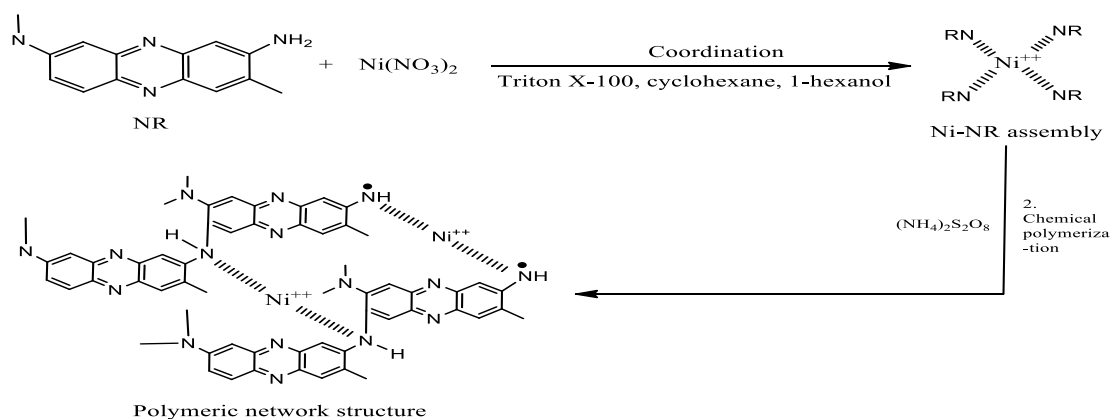
the electrode process was dominated by surface adsorption [39]. At high scan rate of 100~500 $\text{mV}\cdot\text{s}^{-1}$, the peak current i_p was directly proportional to the square root of scan rate $v^{1/2}$ (**Fig.9b**), and the linear regression equation was: $i_{pa} = -4.9724 \times 10^{-6} \cdot v^{1/2} + 2.2794 \times 10^{-5}$ ($R^2 = 0.9991$) and $i_{pc} = 2.7285 \times 10^{-6} \cdot v^{1/2} - 1.4463 \times 10^{-5}$ ($R^2 = 0.9975$). Under high scanning speed condition, the relationships between E_p , i_p and $v^{1/2}$ indicated that the glucose oxidation on the Ni^{2+} @PNR HN/MWCNTs/Nafion modified electrode was a diffusion-confined process [40].

The experiments also investigated the difference between the oxidation peak potential of E_{pa} and the reduction peak potential of E_{pc} , that was, the relationship between the value of ΔE_p ($\Delta E_p = E_{pa} - E_{pc}$) and the scan rate v was also investigated. When the scan rate v was 100 $\text{mV}\cdot\text{s}^{-1}$, the value of ΔE_p between the oxidation peak potential and the reduction peak potential was minimum, so the optimum scan rate was chosen for 100 $\text{mV}\cdot\text{s}^{-1}$.

3.3.2 Selection concentration of Ni^{2+} @PNR HN

The modified electrodes made of Ni^{2+} @PNR HN and MWCNTs/Nafion would be mixed in different proportions, and then were inserted into 0.1 $\text{mol}\cdot\text{L}^{-1}$ NaOH solution or containing 1.0×10^{-7} $\text{mol}\cdot\text{L}^{-1}$ glucose solution. The peak current was defined as the ratio of S/N by CV, and the value of S/N gradually increased with the increase of dilution times. When the dilution ratio was 1:10, the S/N reached its maximum value, so 1:10 was the best dilution factor.

3.4 Possible electrochemical sensing mechanism

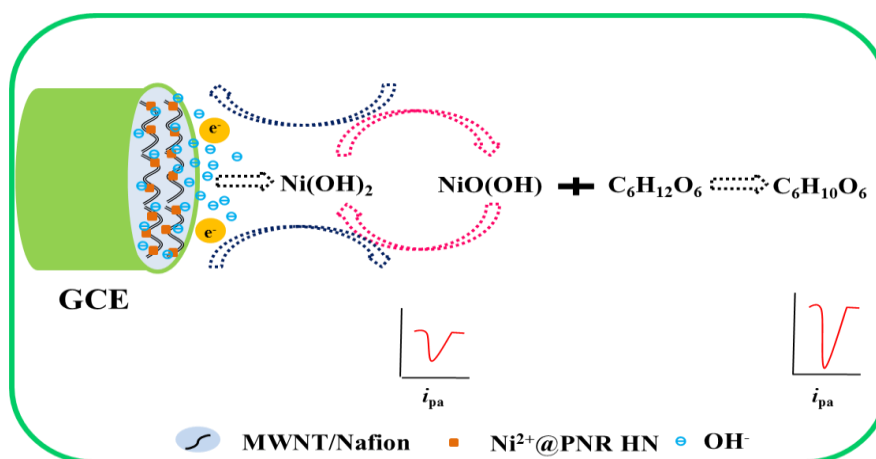


Scheme 1. Block diagram of proposed synthesis of Ni^{2+} @PNR HN materials.

At certain temperatures, the initiator of $\text{K}_2\text{S}_2\text{O}_8$ broke down and produced an active free radical, SO_4^\bullet , which caused the NR monomer to yield free radicals and bound to the NR monomer into dimers or further oligomers. Under the conditions of chemical initiation, NR was more likely to polymerize due to the increase of SO_4^\bullet radicals. When Ni^{2+} was introduced into the process of synthesis of nanocomposites, the N atoms of polymer chains and Ni^{2+} were bonding with the coordinated bonds [41]. Here, PNR provided an excellent support to the Ni^{2+} ion adsorption by its heteroatoms (N), where the electron clouds on the heteroatom interacted with the d-orbital of Ni^{2+} ion

[42]. Accordingly, Ni^{2+} and NR formed a multi-layered, three-dimensional space structure, which greatly enriched the concentration of Ni^{2+} on the modified electrode surface. This made the Ni^{2+} soften and adsorb on the PNR surface which helped to oxidize the Ni^{2+} into $\text{NiO}(\text{OH})$ on the surface of PNR. The formation mechanism of $\text{Ni}^{2+}@PNR$ HN was shown in **Scheme 1**.

The electrocatalytic oxidation characteristics of glucose by $\text{Ni}^{2+}@PNR$ HN can be described as (**Scheme 2**): firstly, the hydroxide ion (OH^-) in the solution diffused toward the modified electrode surface and reacted slowly with Ni^{2+} to form $\text{Ni}(\text{OH})_2$, and the following reaction occurred on the electrode: $\text{Ni}(\text{OH})_2 + \text{OH}^- \rightarrow \text{NiO}(\text{OH}) + \text{H}_2\text{O} + \text{e}^-$, that was, the mutual transformation between $\text{Ni}(\text{OH})_2$ and $\text{NiO}(\text{OH})$. With the addition of glucose, the following chemical reaction occurred: $\text{NiO}(\text{OH}) + \text{glucose} \rightarrow \text{Ni}(\text{OH})_2 + \text{gluconolactone}$, it was accepted that the oxidation of glucose to gluconolactone was catalyzed by the $\text{NiO}(\text{OH})/\text{Ni}(\text{OH})_2$ redox couple, respectively, and therefore the oxidation peak current was increased. The increase of anodic peak current indicated that the oxidation of glucose was accompanied by the electro-oxidation of $\text{Ni}(\text{OH})_2$ to $\text{NiO}(\text{OH})$ [43-45].



Scheme 2. Possible sensing mechanism of electrocatalytic oxidation of glucose by $\text{Ni}^{2+}@PNR$ HN in $0.1 \text{ mol}\cdot\text{L}^{-1}$ NaOH solution.

3.5 Interference experiment

The interferences of common glucose sensor were investigated for $1.0 \times 10^{-6} \text{ mol}\cdot\text{L}^{-1}$ glucose solution with an error of less than $\pm 5\%$, for example, the same concentration of UA, DA and AA, and the experiment results were shown in **Fig.10**. There was no obvious current response observed with the addition of the same concentration of UA, DA and AA. The high selectivity may be attributed to the presence of Nafion, since the negatively charged MWCNTs/Nafion centers repelled UA, DA and AA [16, 46]. It was indicated that the common interferences did not affect the accuracy of the analysis when measuring the glucose concentration.

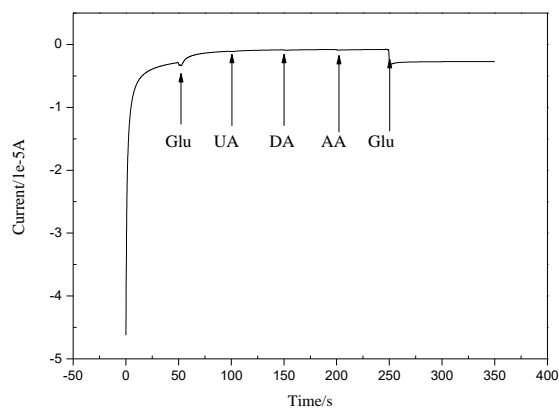


Figure 10. Amperometric responses of the Ni^{2+} @PNR HN/MWCNTs/Nafion modified electrode with successive addition of $1.0 \times 10^{-8} \text{ mol} \cdot \text{L}^{-1}$ Glu, $1.0 \times 10^{-6} \text{ mol} \cdot \text{L}^{-1}$ UA, $1.0 \times 10^{-6} \text{ mol} \cdot \text{L}^{-1}$ DA, $1.0 \times 10^{-6} \text{ mol} \cdot \text{L}^{-1}$ AA and $1.0 \times 10^{-6} \text{ mol} \cdot \text{L}^{-1}$ glucose in $0.1 \text{ mol} \cdot \text{L}^{-1}$ NaOH solution, respectively.

3.6 Analysis characteristics

3.6.1 Linear range and detection limit

The electrocatalytic response of the glucose oxidation on the Ni^{2+} @PNR HN/MWCNTs/Nafion modified electrode was acquired from DPV technique. DPV graphs of Ni^{2+} @PNR HN/MWCNTs/Nafion modified electrodes in $0.1 \text{ mol} \cdot \text{L}^{-1}$ NaOH solution containing different concentrations of glucose were shown in **Fig.11**. With the increase of glucose concentration, the oxidation peak currents of Ni^{2+} @PNR HN/MWCNTs/Nafion modified electrodes were obviously enhanced (**Fig.11A: a**→**j**). In $0.1 \text{ mol} \cdot \text{L}^{-1}$ NaOH solution, the enhanced oxidation peak current of the Ni^{2+} @PNR HN/MWCNTs/Nafion modified electrode and the glucose concentration in the range of $2.0 \times 10^{-8} \text{ mol} \cdot \text{L}^{-1} \sim 1.0 \times 10^{-6} \text{ mol} \cdot \text{L}^{-1}$ showed a good linear relationship (**Fig.11B** and **Fig.11C**). The analytical results were included in **Table 1**.

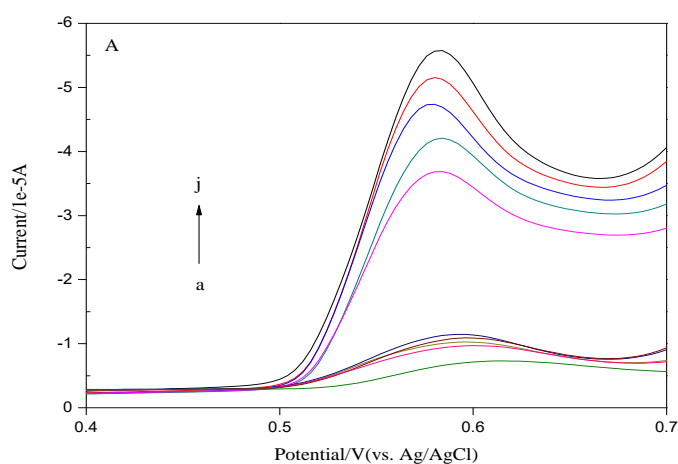


Figure 11. A: DPV curves of different concentration of glucose on the Ni^{2+} @PNR HN/MWCNTs/Nafion modified electrode. (The concentration ranged from a→j, followed by 0 , 2.0×10^{-8} , 4.0×10^{-8} , 6.0×10^{-8} , 8.0×10^{-8} , 1.0×10^{-7} , 3.0×10^{-7} , 5.0×10^{-7} , 7.0×10^{-7} , $1.0 \times 10^{-6} \text{ mol} \cdot \text{L}^{-1}$.)

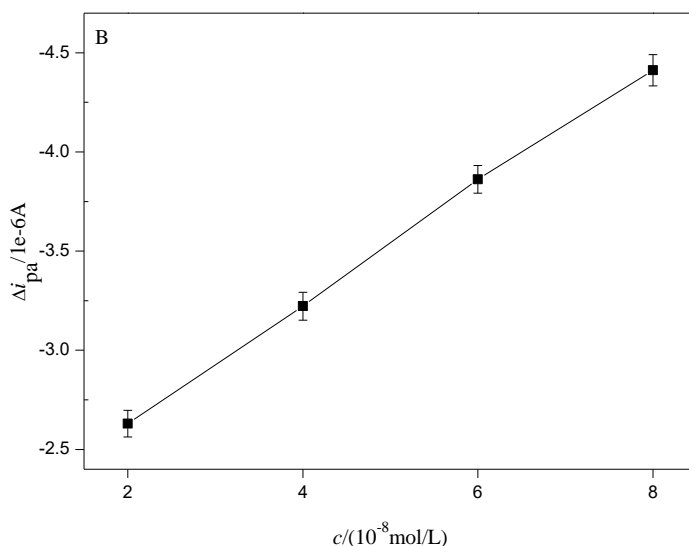


Figure 11. B: The calibration curve of different concentration of glucose on the Ni²⁺@PNR HN/MWCNTs/Nafion modified electrode (the concentration ranged from 2.0×10^{-8} , 4.0×10^{-8} , 6.0×10^{-8} and 8.0×10^{-8} mol·L⁻¹, respectively).

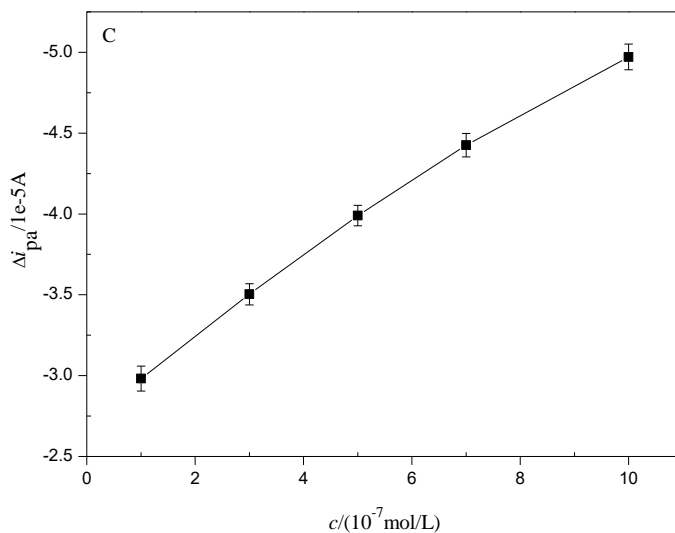


Figure 11. C: The calibration curve of different concentration of glucose on the Ni²⁺@PNR HN/MWCNTs/Nafion modified electrode (the concentration ranged from 1.0×10^{-7} , 3.0×10^{-7} , 5.0×10^{-7} , 7.0×10^{-7} and 1.0×10^{-6} mol·L⁻¹, respectively).

Table 1. Analytical characteristics of the proposed method.

Concentration range (mol·L ⁻¹)	Linear equation (mol·L ⁻¹)	R	RSD % (n=3)	Detection limit ^a (mol·L ⁻¹)
$1.0 \times 10^{-7} \sim 1.0 \times 10^{-6}$	$\Delta i_{pa} / 10^{-5} \text{ A} = -2.2 \times 10^{-6} \cdot c - 2.8$	0.9960	2.5	6.5×10^{-9}
$2.0 \times 10^{-8} \sim 8.0 \times 10^{-8}$	$\Delta i_{pa} / 10^{-6} \text{ A} = -3.0 \times 10^{-7} \cdot c - 2.0$	0.9994		

^a Determined as three times the standard deviation of the blank signals.

For comparison, the performances of other non-enzymatic glucose sensors based on reported in literatures have been listed in **Table 2** [47-55]. As can be seen, the Ni²⁺@PNR HN/MWCNTs/Nafion modified electrode showed a relatively lower detection limit ($6.5 \times 10^{-9} \text{ mol} \cdot \text{L}^{-1}$) compared with others. This phenomenon might be attributing to the special copolymerization structures of Ni²⁺@PNR HN as an active catalytic center, the hybrid nanocomposites containing much more Ni²⁺ and possessing a significant signal amplification effect toward the glucose oxidation reaction, and the effective immobilization of Ni²⁺ at the modified electrode surface. For electrodes of the Cu₅₃@Ni₄₇ CSNPs/rGO [47], Ni@f-MWCNT [49], Ni(OH)₂/NCF [18], NiCo₂S₄ [53], Ni-ZnO [54] and NiNPs/S-BI-PAEK [55], although their linear ranges were wider, the detection limits were more higher than the Ni²⁺@PNR HN/MWCNTs/Nafion modified electrode. Above all, the Ni²⁺@PNR HN/MWCNTs/Nafion modified electrode can be used to fabricate sensor and detect glucose of higher sensitivity over the concentration range from 2.0×10^{-8} to $1.0 \times 10^{-6} \text{ mol} \cdot \text{L}^{-1}$. In addition, our proposed material was synthesized by a simple procedure, and it also showed a reasonable performance when compared with other reports.

Table 2. Comparison of the performances of the proposed sensor with other published non-enzymatic glucose sensors.

Electrode material	Linear range (mol·L ⁻¹)	Detection limit (mol·L ⁻¹)	Reference
Ni ²⁺ @PNR HN	$2.0 \times 10^{-8} \sim 1.0 \times 10^{-6}$	6.5×10^{-9}	This work
Cu ₅₃ @Ni ₄₇ CSNPs/rGO	$1.0 \times 10^{-6} \sim 4.1 \times 10^{-3}$	5×10^{-7}	[47]
Ni(OH) ₂ /N-RGO	$5.0 \times 10^{-7} \sim 1.15 \times 10^{-5}$ $1.15 \times 10^{-5} \sim 2.4 \times 10^{-4}$	1.2×10^{-7}	[15]
Ni(OH) ₂ /NiO nanosheet	$9.0 \times 10^{-5} \sim 1.08 \times 10^{-3}$ $1.08 \times 10^{-3} \sim 3.62 \times 10^{-3}$	5.0×10^{-6}	[48]
Ni@f-MWCNT	$5.0 \times 10^{-5} \sim 1.2 \times 10^{-2}$	2.1×10^{-8}	[49]
Ni(OH) ₂ /NCF	$5 \times 10^{-6} \sim 9.15 \times 10^{-3}$	8×10^{-7}	[18]
Ni(OH) ₂ nanowires	$1 \times 10^{-4} \sim 6 \times 10^{-3}$	1×10^{-6}	[50]
Ni(OH) ₂ /Al(OH) ₄ ⁻	$2.5 \times 10^{-5} \sim 4.5 \times 10^{-4}$	4.76×10^{-5}	[51]
Fe ₃ O ₄ -CNTs-NiNPs	$1 \times 10^{-5} \sim 1.8 \times 10^{-3}$	6.7×10^{-6}	[52]
NiCo ₂ S ₄	$5 \times 10^{-6} \sim 2 \times 10^{-3}$	2×10^{-6}	[53]
Ni-ZnO	$1 \times 10^{-6} \sim 8.1 \times 10^{-3}$	2.8×10^{-7}	[54]
NiNPs/S-BI-PAEK	$1 \times 10^{-6} \sim 4 \times 10^{-3}$	2×10^{-7}	[55]

Notes: NPs: nanoparticles; CSNPs: core-shell nanoparticles; rGO: reduced graphene oxide; N-RGO: nitrogen-doped reduced graphene oxide; Ni@f-MWCNT: Nickel nanoparticles decorated functionalized multi-walled carbon nanotubes; MWCNTs: multiwalled carbon nanotubes; NCF: nitrogen-doped carbon foam; CNTs: carbon nanotubes; S-BI-PAEK: Sulfonate and Benzimidazole functionalized Poly (arylene ether ketone).

3.6.2 Reproducibility and stability property of the Ni²⁺@PNR HN/MWCNTs/Nafion modified electrode

In order to confirm the good reproducibility and stability of the modified electrode, the Ni²⁺@PNR HN/MWCNTs/Nafion modified electrode was placed in $0.1 \text{ mol} \cdot \text{L}^{-1}$ NaOH containing

$1.0 \times 10^{-7} \text{ mol}\cdot\text{L}^{-1}$ glucose solution, and 5 cycles of CV scanning were performed after 72 h. As shown in **Fig.12**, the peak potential of the modified electrode remained essentially unchanged, and the values of the oxidation peak currents were not more than 5 % compared to the first scanning, which clearly confirmed the importance of the MWCNTs/Nafion scaffold in enhancing the stability of Ni^{2+} @PNR HN.

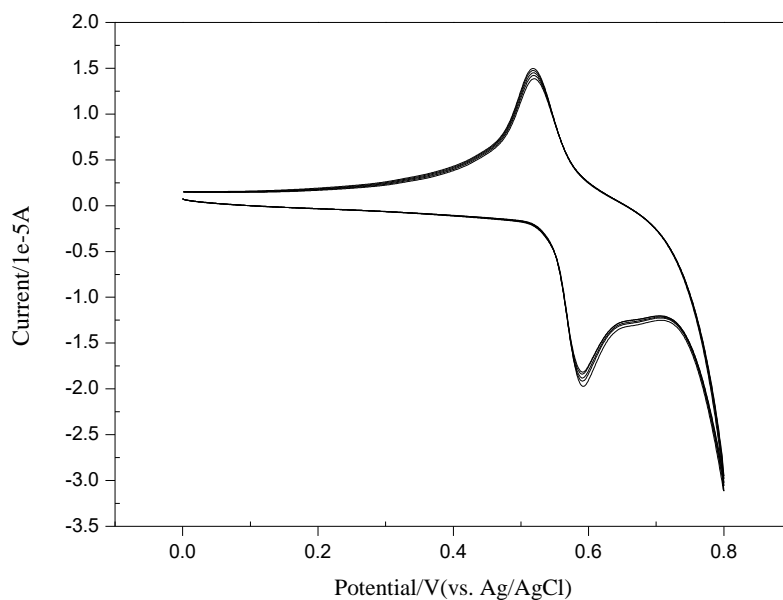


Figure 12. Electrochemical reproducibility and stability of Ni^{2+} @PNR HN/MWCNTs/Nafion modified electrode. ($c_{\text{glucose}} = 1.0 \times 10^{-7} \text{ mol}\cdot\text{L}^{-1}$, $0.1 \text{ mol}\cdot\text{L}^{-1} \text{ NaOH}$, scan rate: $100 \text{ mV}\cdot\text{s}^{-1}$)

3.7 Sample determination

To evaluate the commercial applicability of the proposed glucose sensor, the glucose detection was performed in glucose injection and real biological fluids, such as human serum by DPV method. According to the experimental method, the analysis results of certain concentration of glucose injection were shown in **Table 3**.

Table 3. Determination results of glucose injection.

Sample	Standard ($\text{mol}\cdot\text{L}^{-1}$)	Found ($\text{mol}\cdot\text{L}^{-1}$)	Relative error (% , n=3)
1	5.56×10^{-7}	5.66×10^{-7}	+1.8
2	5.56×10^{-8}	5.35×10^{-8}	-3.8

The standard recovery test with certain amount of human serum by diluted proper multiples was carried out according to the experimental method. Meanwhile, the serum samples without glucose were taken as blank contrast, and the recoveries of glucose concentration from human serum samples were listed in **Table 4**. The proposed glucose sensor received remarkable recovery results from 94.8 %

to 101 %. Hence, the Ni²⁺@PNR HN/MWCNTs/Nafion modified electrode can be potentially used to detect glucose in real samples.

Table 4. Determination results of glucose in serum samples using the proposed glucose sensor (n=3).

Sample	Added (mol·L ⁻¹)	Found ^a (mol·L ⁻¹)	Recovery (%)	RSD ^b (%, n=3)
1	5.0×10 ⁻⁸	1.0×10 ⁻⁸ 5.74×10 ⁻⁸	94.8	3.2
2	6.0×10 ⁻⁷	1.0×10 ⁻⁸ 6.16×10 ⁻⁷	101	3.7

^a Standard deviation method and. ^b Relative standard deviation with three replicative measurements.

4. CONCLUSIONS

Ni²⁺@PNR HN with unique network structure can be synthesized by a facile and one-step reverse microemulsion method. By utilizing the advantages of superstructure nanostructured hybrid material, this very simple method has been proposed to construct a novel non-enzymatic glucose electrochemical sensor. The electrostatic interactions between the positively charged Ni²⁺@PNR HN and the negatively charged MWCNTs/Nafion film, which could become the driving force to assemble Ni²⁺@PNR HN on the modified electrode surface, and provide the effective immobilization of Nickel-based materials in the oxidation of glucose. The proposed enzyme-free glucose sensor has wide linear range, high sensitivity, low detection limit and high response speed, good stability and selectivity, which can be used to detect glucose in human serum samples.

ACKNOWLEDGEMENT

This work was financially supported by the projects from the National Natural Science Foundation of China (No. 21503166) and the Science and Technology Project of Shaanxi Province (No. 2017GY-160).

References

1. J. Wang, *Chem. Rev.*, 108 (2008) 814.
2. S. A. Zaidi, J. H. Shin, *Talanta*, 149 (2016) 30.
3. X. H. Niu, L. B. Shi, H. L. Zhao, M. B. Lan, *Anal. Methods*, 8 (2016) 1755.
4. Z. G. Zhu, L. Garcia-Gancedo, A. J. Flewitt, H. Q. Xie, F. Moussy, W. I. Milne, *Sensors*, 12 (2012) 5996.
5. R. Devasenathipathy, C. Karuppiah, S. M. Chen, S. Palanisamy, B. S. Lou, M. A. Ali, F. M. A. Al-Hemaid, *RSC Adv.*, 5 (2015) 26762.
6. C. C. Gong, J. Y. Chen, Y. H. Song, M. Sun, Y. G. Song, Q. H. Guo, L. Wang, *Anal. Methods*, 8 (2016) 1513.
7. M. Shamsipur, Z. Karimi, M. A. Tabrizi, S. Rostamnia, *J. Electroanal. Chem.*, 799 (2017) 406.
8. N. Jadon, R. Jain, S. Sharma, K. Singh, *Talanta*, 161 (2016) 894.

9. G. Q. Liu, H. Zhong, X. R. Li, K. Yang, F. F. Jia, Z. P. Cheng, L. L. Zhang, J. Z. Yin, L. P. Guo, H. Y. Qian, *Sensor. Actuat. B*, 242 (2017) 484.
10. L. Shabnam, S. N. Faisal, A. K. Roy, E. Haque, A. I. Minett, V. G. Gomes, *Food Chemistry*, 221 (2017) 751.
11. Y. Zhang, F. Xu, Y. Sun, Y. Shi, Z. Wen, Z. Li, *J. Math. Chem.*, 21 (2011) 16949.
12. P. Si, Y. Huang, T. Wang, J. Ma, *RSC Adv.*, 3 (2013) 3487.
13. C. M. Welch, R. G. Compton, *Anal. Bioanal. Chem.*, 384 (2006) 601.
14. G. Başkaya, Y. Yıldız, A. Savk, T. O. Okyay, S. Eriş, H. Sert, F. Şen, *Biosens. Bioelectron.*, 91 (2017) 728.
15. Y. H. Zhang, W. Lei, Q. J. Wu, X. F. Xia, Q. L. Hao, *Microchim. Acta*, 5 (2017) 1.
16. S. J. Li, W. Guo, B. Q. Yuan, D. J. Zhang, Z. Q. Feng, J. M. Du, *Sensor. Actuat. B*, 240 (2017) 398.
17. K. Ramachandran, T. R. Kumar, K. J. Babu, G. G. Kumar, *Scientific Reports*, 6 (2016) 36583.
18. Q. H. Guo, M. Zhang, S. W. Liu, G. Y. Zhou, X. Li, H. Q. Hou, L. Wang, *Anal. Methods*, 8 (2016) 8227.
19. B. Zhao, X. K. Ke, J. H. Bao, C. L. Wang, L. Dong, Y. W. Chen, H. L. Chen, *J. Phys. Chem. C*, 113 (2009) 14440.
20. W. Huang, Y. Cao, Y. Chen, J. Peng, X. Y. Lai, J. C. Tu, *Appl. Surf. Sci.*, 396 (2017) 804.
21. M. do S. M. Quintino, H. Winnischofer, M. Nakamura, K. Araki, H. E. Toma, L. Angnes, *Anal. Chim. Acta*, 539 (2005) 215.
22. X. Y. Wang, Y. Zhang, C. E. Banks, Q. Y. Chen, X. B. Ji, *Colloid. Surface. B: Biointerfaces*, 78 (2010) 363.
23. E. Scavetta, S. Stipa, D. Tonelli, *Electrochem. Commun.*, 9 (2007) 2838.
24. M. Mazloum-Ardakani, E. Amin-Sadrabadi, A. Khoshroo, *J. Electroanal. Chem.*, 775 (2016) 116.
25. T. Liu, Y. Q. Luo, J. M. Zhu, L. Y. Kong, W. Wang, L. Tan, *Talanta*, 156-157 (2016) 134.
26. F. Cao, S. Guo, H. Y. Ma, D. Shan, S. X. Yang, J. Gong, *Biosens. Bioelectron.*, 26 (2011) 2756.
27. Z. J. Deng, H. Y. Long, Q. P. Wei, Z. M. Yu, B. Zhou, Y. J. Wang, L. Zhang, S. S. Li, L. Ma, Y. N. Xie, J. Min, *Sensor. Actuat. B*, 242 (2017) 825.
28. A. Salimi, M. Roushani, *Electrochem. Commun.*, 7 (2005) 879.
29. P. M. Ajayan, *Chem. Rev.*, 99 (1999) 1787-1800.
30. L. Agüí, P. Yáñez-Sedeño, J. M. Pingarrón, *Anal. Chim. Acta*, 622 (2008) 11.
31. A. Lehmani, P. Turq, M. Périé, J. Périé, J. P. Simonin, *J. Electroanal. Chem.*, 428 (1997) 81.
32. Z. H. Guo, S. J. Dong, *Anal. Chem.*, 76 (2004) 2683.
33. J. P. Choi, A. J. Bard, *J. Electroanal. Chem.*, 573 (2004) 215.
34. R. Pauliukaite, C. M. A. Brett, *Electroanalysis*, 20 (2008) 1275.
35. Y. Y. Zhang, R. Yuan, Y. Q. Chai, Y. Xiang, C. L. Hong, X. Q. Ran, *Biochem. Eng. J.*, 51 (2010) 102.
36. I. Tiwari, M. Gupta, *Mater. Res. Bull.*, 49 (2014) 94.
37. C. M. Yang, J. L. Yi, X. J. Tang, G. Z. Zhou, Y. Zeng, *React. Funct. Polym.*, 66 (2006) 1336.
38. C. Z. Zhao, C. L. Shao, M. H. Li, K. Jiao, *Talanta*, 71 (2007) 1769.
39. X. L. Wang, E. L. Liu, X. L. Zhang, *Electrochim. Acta*, 130 (2014) 253.
40. L. Wang, Y. Z. Xie, C. T. Wei, X. P. Lu, X. Li, Y. H. Song, *Electrochim. Acta*, 174 (2015) 846.
41. S. K. Shukla, M. M. Demir, P. P. Govender, A. Tiwari, S. K. Shukla, *Sensor. Actuat. B*, 242 (2017) 522.
42. K. E. Toghill, R. G. Compton, *Int. J. Electrochem. Sci.*, 5 (2010) 1246.
43. W. D. Zhang, J. Chen, L. C. Jiang, Y. X. Yu, J. Q. Zhang, *Microchim. Acta*, 168 (2010) 259.
44. Y. Jiang, S. Yu, J. Li, L. Jia, C. Wang, *Carbon*, 63 (2013) 367.
45. K. D. Xia, C. Yang, Y. L. Chen, L. L. Tian, Y. Y. Su, J. B. Wang, L. Li, *Sensor. Actuat. B*, 240 (2017) 979.
46. S. Hrapovic, Y. L. Liu, K. B. Male, J. H. T. Luong, *Anal. Chem.*, 76 (2004) 1083.

47. K. L. Wu, Y. M. Cai, B. B. Jiang, W. C. Cheong, X. W. Wei, W. Z. Wang, N. Yu, *RSC Adv.*, 7 (2017) 21128.
48. W. Huang, L. Y. Ge, Y. Chen, X. Y. Lai, J. Peng, J. C. Tu, Y. Cao, X. T. Li, *Sens. Actuators B*, 248 (2017) 169.
49. G. Başkaya, Y. Yıldız, A. Savk, T. O. Okyay, S. Eriş, H. Sert, F. Şen, *Biosens. Bioelectron.*, 91 (2017) 728.
50. Q. Xiao, X. X. Wang, S. P. Huang, *Mater. Lett.*, 198 (2017) 19.
51. M. Jarosz, R. P. Socha, P. Józwik, G. D. Sulka, *Appl. Surf. Sci.*, 408 (2017) 96.
52. N. Nontawong, M. Amatatongchai, P. Jarujamrus, S. Tamuang, S. Chairam, *Int. J. Electrochem. Sci.*, 12 (2017) 1362.
53. D. L. Chen, H. Y. Wang, M. H. Yang, *Anal. Methods*, 9 (2017) 4718.
54. Y. Yang, Y. L. Wang, X. Y. Bao, H. C. Li, *J. Electroanal. Chem.*, 775 (2016) 163.
55. L. L. Xi, T. F. Wang, D. W. Zhang, *Electroanalysis*, 29 (2017) 1.

© 2018 The Authors. Published by ESG (www.electrochemsci.org). This article is an open access article distributed under the terms and conditions of the Creative Commons Attribution license (<http://creativecommons.org/licenses/by/4.0/>).